

The Generation and Trapping of Solitary Waves over Topography

David Farmer and Laurence Armi

Observations of tidal flow over a sill show that upstream solitary wave generation occurred in conjunction with the downstream movement of a streamline bifurcation over the obstacle crest. Solitary waves appeared upstream of the bifurcation, riding on the surface stratification. Shear flow instabilities on the plunging interface were also evident and may contribute to wave generation through subharmonic interaction. Nonlinear waves generated downstream of an internal control became trapped in the supercritical flow.

Internal solitary waves are a widespread and prominent feature in oceans (1), lakes (2), and the atmosphere (3). Satellite images of the ocean reveal their distribution and propagation, but generation mechanisms have not been well documented. Internal solitary waves influence mixing, acoustic propagation, radar observations, and offshore engineering design. They may arise from the relaxation of internal hydraulic flows (4), the release of internal lee waves (5), intrusions created by collapsing mixed layers (6), and upstream influence (7). We report observations illustrating further mechanisms that may be responsible for their generation.

Our measurements were made in Knight Inlet, British Columbia, Canada (Fig. 1, inset), a 90-km-long density-stratified fjord with a 60-m sill separating two deep basins. Measurements included towed and profiling temperature/salinity sensors, acoustic Doppler and echo-sounder imaging, and aerial photographs. The solitary waves can be seen as a surface modulation resulting from variations in both the gravity-capillary wave field and thickness of the sediment-laden surface layer (Fig. 1A) and can also be acoustically detected (Fig. 1B). Typically, the waves form almost straight lines, consistent with the two-dimensional behavior of the flow near the channel center. Similar surface patterns are widely observed in satellite radar images over continental shelves (8).

When the tidal current accelerates over the sill, the near-surface streamlines bifurcate at a depth of ~ 5 m, followed by a steeply inclined and unstable flow as the weakly stratified deeper layer plunges down the lee face of the sill in a manner reminiscent of severe downslope mountain winds (9). The bifurcation normally occurs well upstream of

the crest, but it can be pushed downstream in strong tidal currents.

Although we could not detect the moment of wave generation, the mechanism appears linked to the temporal evolution of the bifurcation, in which the waves radiate upstream as the bifurcation is forced downstream by the tidal current. The interfacial waves evolved to form narrow, steep-sided depres-

sions in the shallow stratification (Fig. 1B). In this and other similar examples, the waves were formed as the bifurcation moved downstream over the sill crest. The flow is controlled at the sill crest, and the waves occur in the subcritical portion (that is, $x < 0$) of the flow upstream of the crest.

Preceding formation of the waves, we always observed interfacial instabilities beginning well upstream of the sill crest (Fig. 2A). The corresponding wavelength increased rapidly downstream, and small-scale structure was superimposed on larger scale features, which is indicative of subharmonic interaction (Fig. 2A, inset). Approximately 30 min later (Fig. 2B), the overall interface shape remained similar, but interfacial waves ($\lambda = 50$ to 100 m) appeared near the unstable flow, and nonlinear waves had formed upstream. Subsequent traverses showed that the bifurcation was pushed downstream by the increasing tidal current until it approached, but did not quite reach, the shape shown in Fig. 1B. Thus, the waves in Fig. 2B were formed before major changes in the interface shape; therefore, we investigate the potential role of interfacial instabilities in wave generation.

The stability and speed of linear interfa-

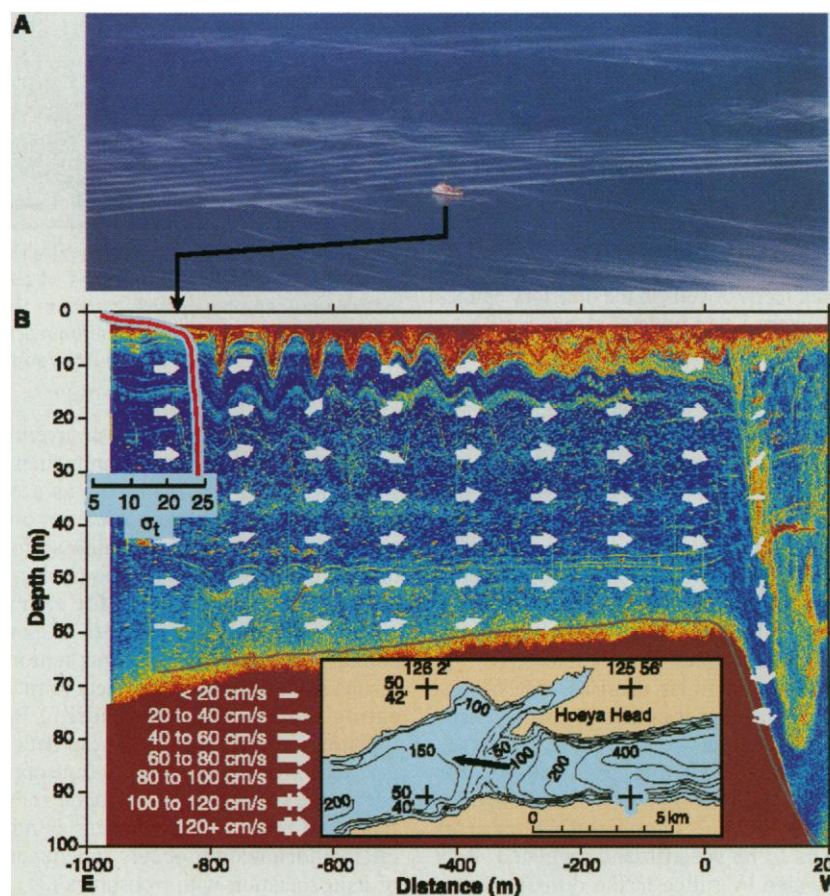


Fig. 1. (A) Aerial photograph showing the C.S.S. Vector about to traverse a group of solitary waves over the sill in Knight Inlet, British Columbia, 0212 UTC on 28 August 1995. (B) Corresponding echo-sounding image of solitary waves. Arrows indicate current vectors shown at same aspect ratio as figure and coded as to magnitude. (Top left) Upstream density profile in σ_t . (Inset) Chart of sill area with arrow showing ship track.

D. Farmer, Institute of Ocean Sciences, Post Office Box 6000, Sidney, BC V8L 4B2, Canada (E-mail: farmerd@dfp-mpo.gc.ca). L. Armi, Scripps Institution of Oceanography, La Jolla, CA 92093-0230, USA (larmi@ucsd.edu).

REPORTS

cial waves is given by the relevant dispersion relationship (10)

$$c(k) = \frac{\{k[U_1 R_1 + U_2 R_2] \pm \sqrt{k^2[U_1 R_1 + U_2 R_2]^2 - \Sigma R[U_1^2 k^2 R_1 + U_2^2 k^2 R_2 - \rho_2 g' k]}\}}{k \Sigma R} \quad (1)$$

where U_i is the speed, ρ_i is the density, and h_i is the thickness of the upper and lower layers (with $i = 1$ and 2 , respectively), k is the wavenumber, $R_i = \rho_i \cotanh(kh_i)$, $\Sigma R = R_1 + R_2$, g is gravitational acceleration, and $g' = g(\rho_2 - \rho_1)/\rho_2$ is the reduced gravity. The bulk properties of the steady topographic response are well approximated by the hydraulic equations (11), which confirm that the flow is controlled ($F_1^2 + F_2^2 = 1$, where $F_i^2 = U_i^2/g'h$) at the sill crest. Linear waves are arrested when the wave speed is zero and are unstable when it is complex. Equation 1 may be solved to determine dispersion characteristics as a function of position. Positive and negative roots correspond to waves propagating with and against the flow. For waves traveling against the flow, long waves are arrested at the crest. Downstream of the crest, all infinitesimal waves are lost, whereas upstream of this location sufficiently long waves can escape. Waves propagating upstream move along an interface that becomes progressively shallower and less sheared, with an evolution expected to be similar to surface waves propagating toward a beach (12).

The dispersion relationship (Eq. 1) corresponding to Fig. 2A is shown in Fig. 2C, in which the stability boundary and speeds of upstream propagating internal waves are shown as a function of position x and wavenumber k . Upstream of the crest, the flow is subcritical ($F_1^2 + F_2^2 < 0.2$ for $x = -800$ m), so that long waves always escape, but under the competing effects of changing layer depths, shear, and density stratification, their speed passes through a maximum before approaching uniform upstream conditions. Only high wavenumbers are unstable, and these must all travel downstream. The speeds of finite amplitude interfacial waves (dashed curves in Fig. 2C) always exceed c_0 and increase with amplitude.

Although upstream wave generation can be demonstrated as a solution to the KdV and related equations, a possible alternative generation mechanism involves the bifurcation of stratified flows and the resultant development of instabilities. This mechanism, illustrated as a number sequence (Fig. 2C, red dots), begins with a small-scale instability ("1") that grows rapidly. Subharmonic generation is known to occur in unstable shear layers (13) and appears to be present here (Fig. 2A, inset), creating longer interfacial disturbances, some of which propagate upstream ("2" \rightarrow "3"). Even if waves just upstream of the unstable flow are initially linear, they can be expected to become nonlinear as they move along the shoaling interface ("3" \rightarrow "4"). The result ("4") is a sequence of

solitary waves. Slowed by the topographically accelerated background flow, they gradually advance upstream.

Nonlinear waves formed upstream of the crest are free to escape ("A" in Fig. 2C), but those formed downstream of the crest may

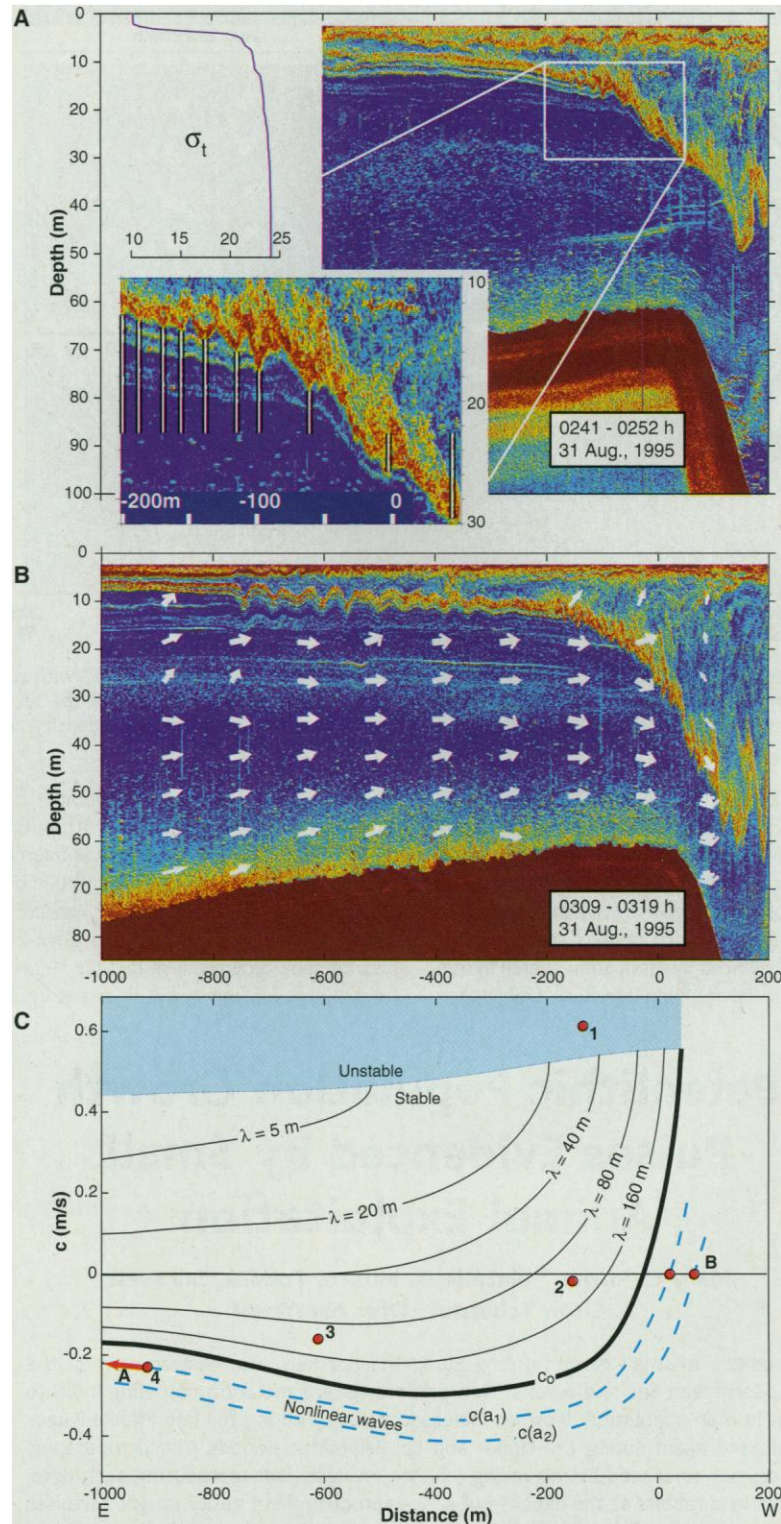


Fig. 2. (A) (Top left) Upstream density profile in σ_t . (Right) Echo-sounding image of downstream traverse showing unstable interface. (Inset) Vertical lines identify instability scale. (B) Repeat traverse traveling upstream approximately 30 min after (A). (C) Dispersion diagram for internal waves applicable to (A) propagating against the current. Dashed curves represent nonlinear waves (not modeled). Blue shading indicates unstable flow. "1" \rightarrow "2" (red dots) represents subharmonic formation of longer waves from instabilities; "2" \rightarrow "3" represents linear propagation; "3" \rightarrow "4" represents transition to nonlinearity.

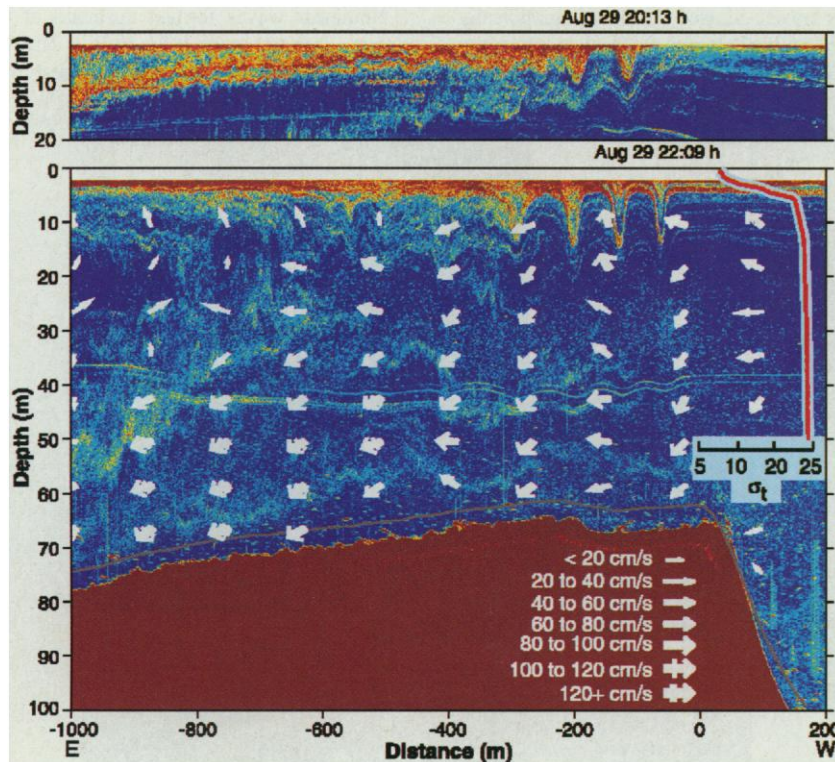


Fig. 3. Echo soundings of solitary waves formed above the sill crest during a flood tide, with current vectors. The waves are trapped just downstream of the internal hydraulic control at the sill crest. The upper image was made 2 hours before the lower image. (Top right) Upstream density profile.

become trapped (“B”) in the supercritical flow ($F_1^2 + F_2^2 > 1$). Trapping is more readily observed over the gentler lee slope during flood tide. The waves in Fig. 3 were trapped for more than 2 hours. Trapped waves maintain their amplitude for extended periods, implying that growth is balanced by dissipation, which in turn determines the trapping location. Only when

the tidal current decreases and hydraulic control is lost do they escape upstream. Amplification of waves moving up the subcritical interface as in Fig. 2B, and the resultant amplitude dispersion as they become nonlinear, ensures that waves formed in the subcritical flow tend to become rank ordered, such that the largest is in front. However, this result does not apply for

trapped waves, because the convective speed $u_{conv} = (u_1 h_2 + u_2 h_1)/(h_1 + h_2)$ increases with distance downstream. Trapped solitary waves are therefore reverse rank ordered, as may be seen for the leading waves in Fig. 3.

Although the changing background current must be considered in any detailed model of stratified flow over topography, our observations show that such flows can be quite unstable, and this instability may play a role in the generation of internal solitary waves which propagate upstream or become trapped downstream of the control.

References and Notes

1. A. R. Osborne and T. L. Burch, *Science* **208**, 451 (1980).
2. D. Farmer, *J. Phys. Oceanogr.* **8**, 63 (1978).
3. R. J. K. Smith, N. Crook, G. Roff, *Q. J. R. Meteorol. Soc.* **108**, 937 (1982).
4. J. R. Apel, J. R. Holbrook, A. K. Liu, J. J. Tsai, *J. Phys. Oceanogr.* **15**, 1625 (1985); T. Maxworthy, *J. Geophys. Res.* **84**, 338 (1979).
5. C.-Y. Lee and R. C. Beardsley, *J. Geophys. Res.* **79**, 453 (1974); D. Farmer and D. Smith, *Deep-Sea Res.* **27A**, 239 (1980).
6. T. Maxworthy, *J. Fluid Mech.* **96**, 47 (1980).
7. P. G. Baines, *ibid.* **146**, 127 (1984); R. H. J. Grimshaw and N. Smyth, *ibid.* **169**, 429 (1986); W. K. Melville and K. R. Helfrich, *ibid.* **178**, 31 (1987); J. Grue, H. A. Friis, E. Palm, P. O. Rusan, *ibid.* **351**, 223 (1997).
8. A. K. Liu *et al.*, *J. Geophys. Res.* **103**, 7995 (1998).
9. D. M. Farmer and L. Armi, *Proc. R. Soc. London Ser. A*, in press.
10. S. A. Thorpe, *J. Fluid Mech.* **85**, 7 (1978).
11. L. Armi, *ibid.* **163**, 27 (1986); see Eqs. 10a–d.
12. P. Liu, in *Ocean Engineering Science*, vol. 9 of *The Sea*, B. Le Méhauté and D. M. Hanes, Eds. (Wiley, New York, 1990), pp. 27–63.
13. C. D. Winant and F. K. Browand, *J. Fluid Mech.* **63**, 237 (1974); G. Pawlak and L. Armi, *ibid.* **376**, 1 (1998).
14. We are indebted to the officers and crew of the C.S.S. *Vector* for their assistance, K. Bartlett and N. Hulbirt for assistance with processing, and M. Li for helpful discussion. Funded under the U.S. Office of Naval Research program on internal solitary waves.

21 August 1998; accepted 18 November 1998

Paleolithic Population Growth Pulses Evidenced by Small Animal Exploitation

Mary C. Stiner,* Natalie D. Munro, Todd A. Surovell, Eitan Tchernov, Ofer Bar-Yosef

Variations in small game hunting along the northern and eastern rims of the Mediterranean Sea and results from predator-prey simulation modeling indicate that human population densities increased abruptly during the late Middle Paleolithic and again during the Upper and Epi-Paleolithic periods. The demographic pulses are evidenced by increasing reliance on agile, fast-reproducing partridges, hares, and rabbits at the expense of slow-reproducing but easily caught tortoises and marine shellfish and, concurrently, climate-independent size diminution in tortoises and shellfish. The results indicate that human populations of the early Middle Paleolithic were exceptionally small and highly dispersed.

The size of a population has much to do with its long-term prospects for survival and the potential impact of random events on its evo-

lutionary history. It is difficult to appreciate or quantify just how small early Paleolithic populations were or how thinly they were

spread during much of the Pleistocene. Thus, to assess when human populations grew during the Late Pleistocene, we analyzed trends in the small animal species most commonly eaten by Paleolithic foragers.

Paleolithic humans relied on both small animals and ungulates for meat (1), but predator-prey relations between humans and small animals are more sensitive indicators of changes in human population density (2) because small prey species vary much more than ungulate species with respect to life history and predator avoidance characteristics. In the Mediterranean Basin (Israel and

M. C. Stiner, N. D. Munro, T. A. Surovell, Department of Anthropology, Building 30, University of Arizona, Tucson, AZ 85721, USA. E. Tchernov, Department of Evolution, Systematics and Ecology, The Hebrew University of Jerusalem, Jerusalem 91904, Israel. O. Bar-Yosef, Department of Anthropology, Peabody Museum, Harvard University, Cambridge, MA 02138, USA.

*To whom correspondence should be addressed. E-mail: mstiner@u.arizona.edu